

Supporting Information for

A Fe-Ni₅P₄/Fe-Ni₂P Heterojunction Electrocatalyst for Highly-Efficient Solar-to-Hydrogen Generation

Rui Zhang,^{a,b} Guodong Wang,^b Zhenhua Wei,^a Xue Teng,^c Jiejie Wang,^c Jiaojiao Miao,^b Yuheng, Wang,^b Fangxu Yang,^c Xiangwei Zhu,^{b*} Changfeng Chen,^c Erjun Zhou,^b Wenping Hu,^{e*} and Xiangnan Sun^{a,b,d*}

^a Shandong First Medical University & Shandong Academy of Medical Sciences, Taian 271016, China

^b Key Laboratory of Nanosystem and Hierarchical Fabrication, CAS Center for Excellence in Nanoscience, National Center for Nanoscience and Technology, Beijing 100190, China

^c Department of Materials Science and Engineering, College of Science, China University of Petroleum, Beijing 102249, China

^d School of Material Science and Engineering, Zhengzhou University, Zhengzhou 450001, China.

^e Tianjin Key Laboratory of Molecular Optoelectronic Science, Department of Chemistry, School of Science, Tianjin University & Collaborative Innovation Center of Chemical Science and Engineering (Tianjin), Tianjin 300072, China

*Corresponding Author

E-mail: zhuxw@nanoctr.cn

E-mail: sunxn@nanoctr.cn

E-mail: huwp@tju.edu.cn

Experimental Section

Materials

All the reagents for synthesis are analytical grade and used without further purification. The commercial Pt and RuO₂ electrodes (electroplated on Ti mesh) are provided by Baoji Zhiming Special Metal Co., LTD (China) [Tel.86-0917-3122785; <http://www.zmanode.com>].

Synthesis processes

A piece of nickel foam (NF) ($1 \times 3 \text{ cm}^2$) is washed with 0.5 M HCl, ethanol and deionized water successively to remove the surface oxide layer, and then immersed into a 35 mL aqueous solution containing 2 mmol Ni(NO₃)₂+FeSO₄, 10 mmol NH₄F and 25 mmol urea. The mole ratios of Ni:Fe are kept as 9:1, 3:1, 1:1, 1:3 and 1:9 in this work. The aqueous solution with the NF is transferred to a 50 mL Teflon-lined stainless-steel autoclave and heated at 120 °C for 16 h. After cooling to room temperature, the NF with precursor is washed with deionized water several times and vacuum dried at 60 °C. To prepare the phosphides, NaH₂PO₂·H₂O is placed at the upstream side of the tube furnace and the NF with precursor placed at the downstream side. Then, the samples are heated at 400 °C for 120 min with a heating rate of 3 °C min⁻¹ in H₂/Ar (10%/90%) gas flowing at 200 s.c.c.m. to obtain H-FeNiP. A-FeNiP is synthesized by the similar method in Ar atmosphere. To prepare H-FeNiP on carbon felt (CF), a piece of CF ($1 \times 3 \text{ cm}^2$) is treated with concentrated HNO₃ for 1 h firstly, and then washed with deionized water three times under ultrasonic condition. The following processes are the same as the preceding method, in which the mole ratios of Ni:Fe is fixed at 3:1. NiP is synthesized without adding any Fe source, while NF-P is synthesized by directly using NF as the precursor.

Characterizations

X-ray powder diffraction (XRD) data are obtained on a D/MAX 2500 diffractometer (Rigaku, Japan) with Cu K α radiation ($\lambda = 1.54178 \text{ \AA}$). Scanning electron microscopy (SEM) images are taken on a Hitachi S-4800N field emission scanning electron microscopy (Hitachi, Japan). The transmission electron microscopy (TEM), the high-resolution TEM (HRTEM) and the corresponding elemental mapping analyses are performed on a Tecnai G2 F20 U-TWIN transmission electron microscopy (FEI, America). X-ray photoelectron spectra (XPS) are obtained on an ESCALAB MK II X-ray photoelectron spectrometer with Mg K α as the excitation source.

Electrochemical Measurements

Electrochemical tests are performed with a CHI 760E electrochemistry workstation (CH Instruments, Inc., Shanghai) in a standard three-electrode system at $25 \pm 1 \text{ }^\circ\text{C}$ using 1 M KOH as the electrolyte, electrocatalyst on substrate as the working electrode, Ag/AgCl electrode as the reference electrode and Pt (for OER) or carbon (for HER) as the counter electrode. All potentials reported are calibrated to reversible hydrogen electrode (RHE) by $E(\text{RHE}) = E(\text{Ag/AgCl}) + 0.197 \text{ V} + 0.059 \times \text{pH}$ and the current densities (j) are normalized by geometric surface area. The polarization curves are corrected against ohmic potential drop if not specified. Drainage method is used to determine the Faradic efficiency. For the solar-driven water-splitting experiment, the electrolytic cell is in series with a PTB7-Th/PC₇₁BM/CO_i8DFIC (or P3HT/PCBM) solar cell and an electrochemistry workstation. The simulated sunlight is produced by XES 200S1 (AM 1.5G 100 mW·cm⁻², SAN-EI ELECTRIC CO., LTD., Japan) and the current density of the water splitting cell is recorded by chronoamperometry without applied electrical potential.

Computational Methods

The present first principle DFT calculations are performed with the projector augmented wave (PAW) method (*Phys. Rev. B* **1999**, *59*, 1758). The exchange-functional is treated using the generalized gradient approximation (GGA) of Perdew-Burke-Ernzerhof (PBE) functional (*Phys. Rev. Lett.* **1996**, *77*, 3865). The cut-off energy of the plane-wave basis is set at 450 eV for optimize calculations of atoms and cell optimization. The Brillouin zone integration is performed using $3 \times 3 \times 1$ Monkhorst-Pack k-point sampling for a primitive cell (*Phys. Rev. B* **1977**, *16*, 5188). The van der Waals (vdW) interactions were considered using the DFT-D2 method of Grimme (*J. Comput. Chem.* **2006**, *27*, 1787). The self-consistent calculations apply a convergence energy threshold of 10^{-5} eV. The vacuum spacing in a direction perpendicular to the plane of the catalyst is at least 15 Å to avoid the spurious interactions of neighboring models. The equilibrium lattice constants are optimized with maximum stress on each atom within 0.05 eV/Å. The Hubbard U (DFT+U) corrections for 3d transition metal by setting according to the literature (*Adv. Energy Mater.* **2019**, *9*, 1902625), for which the nickel 3d and 4s electrons, iron 3d and 4s electrons, phosphorus 3s and 3p electrons, hydrogen 1s electron and oxygen 2s and 2p electrons are treated as valence electrons.

In our model, the Ni₅P₄ (001) slab has been obtained from the bulk Ni₅P₄ crystal structure (P63mc space group) with the lattice parameters (a=b=6.7786 Å). In addition, the Ni₂P (001) slab with the lattice parameters (a=b=5.86 Å) has been obtained from the bulk Ni₂P crystal structure (P-62m space group). We fully optimize the slab structures with the bottom two layers fixed. Finally, the interface model is constructed by the slab model of both $2 \times 2 \times 1$ supercell of Ni₂P and Ni₅P₄ (001) slab with the lattice parameters (a=b=12.64 Å, b=23.11 Å). In our

calculation, we fix the supercell parameters and relax the atoms in our interface structure with bottom two layers fixed, which generating 8.56% and 9.63% mechanical strains at the interface of Fe-Ni₅P₄/Fe-Ni₂P and NiFe-LDH/Fe-Ni₂P, respectively. A similar method of building an interface model was also reported previously (*Chem. Mater.* **2014**, *26*, 4248; *Nano Energy* **2020**, *68*, 104332).

The free energy was calculated using the equation:

$$G = E + ZPE - TS$$

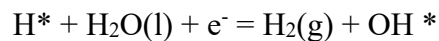
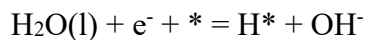
where G , E , ZPE and TS are the free energy, total energy from DFT calculations, zero-point energy and entropic contributions (T was set to be 300 K), respectively. ZPE could be derived after frequency calculation by (*J. Chem. Phys. B* **2004**, *108*, 17886):

$$ZPE = \frac{1}{2} \sum h\nu_i$$

And the TS values of adsorbed species are calculated after obtaining the vibrational frequencies (*J. Phys. Chem. C* **2013**, *117*, 26048):

$$TS_v = k_B T \left[\sum_K \ln\left(\frac{1}{1-e^{-hv/k_B T}}\right) + \sum_K \frac{hv}{k_B T} \frac{1}{(e^{hv/k_B T} - 1)} + 1 \right]$$

The free energy of HER in alkaline has been calculated by considering the following sequential steps, where * denotes surface sites (*Adv. Mater.* **2020**, *32*, 1906972):



The OER process in alkaline medium generally occur through the following steps

(*ChemCatChem* **2011**, *3*, 1159):



The potential determining step in OER is estimated by the magnitude of G^{OER} , which is

defined as:

$$G^{\text{OER}} = \max[\Delta G_1^0, \Delta G_2^0, \Delta G_3^0, \Delta G_4^0]$$

where ΔG_{1-4}^0 is ΔG_{1-4} at $U=0$.

The theoretical overpotential at standard conditions is then given by:

$$\eta^{\text{OER}} = (G^{\text{OER}}/\text{e}) - 1.23 \text{ V}$$

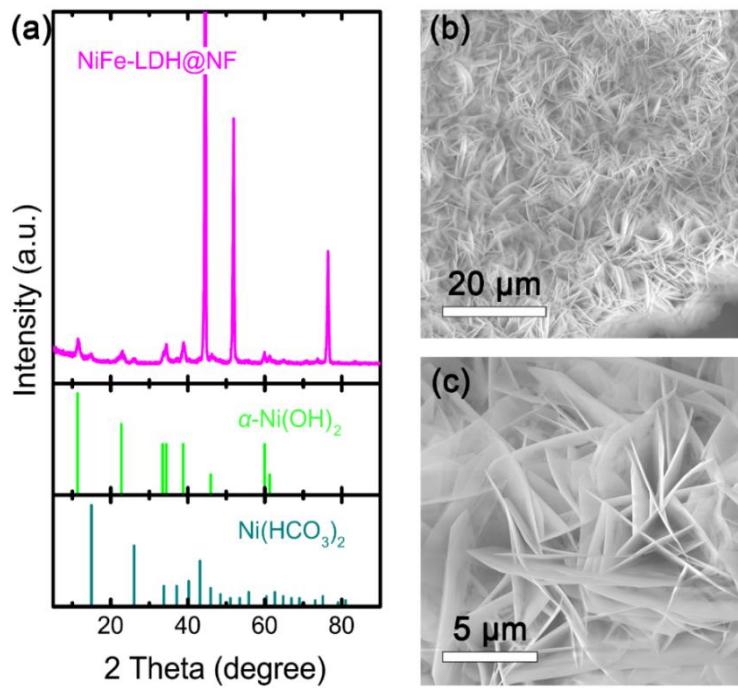


Fig. S1. (a) The XRD pattern. (b) Low and (c) high magnification SEM images. The synthesized NiFe-LDH on NF shares similar structure with α -Ni(OH)₂ (PDF No. 38-0715), while some weak peaks at $2\theta = 14.9^\circ$, 26.1° and 37.1° can also be observed, which match well with Ni(HCO₃)₂ (PDF No. 15-0782).

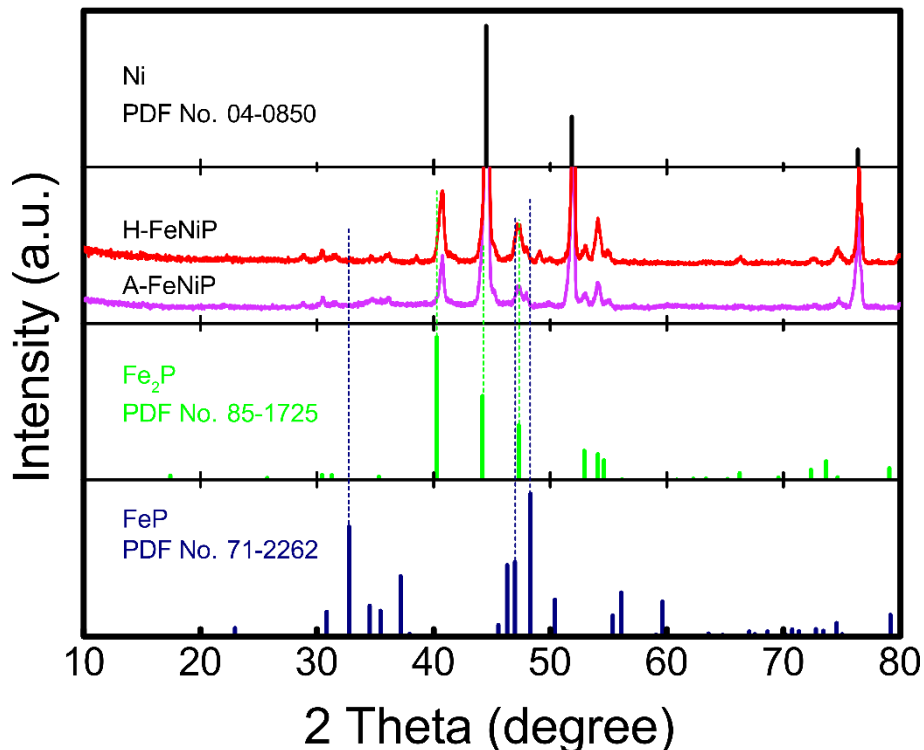


Fig. S2. XRD patterns of A-FeNiP and H-FeNiP along with the standard diffraction patterns of Fe₂P, FeP and Ni.

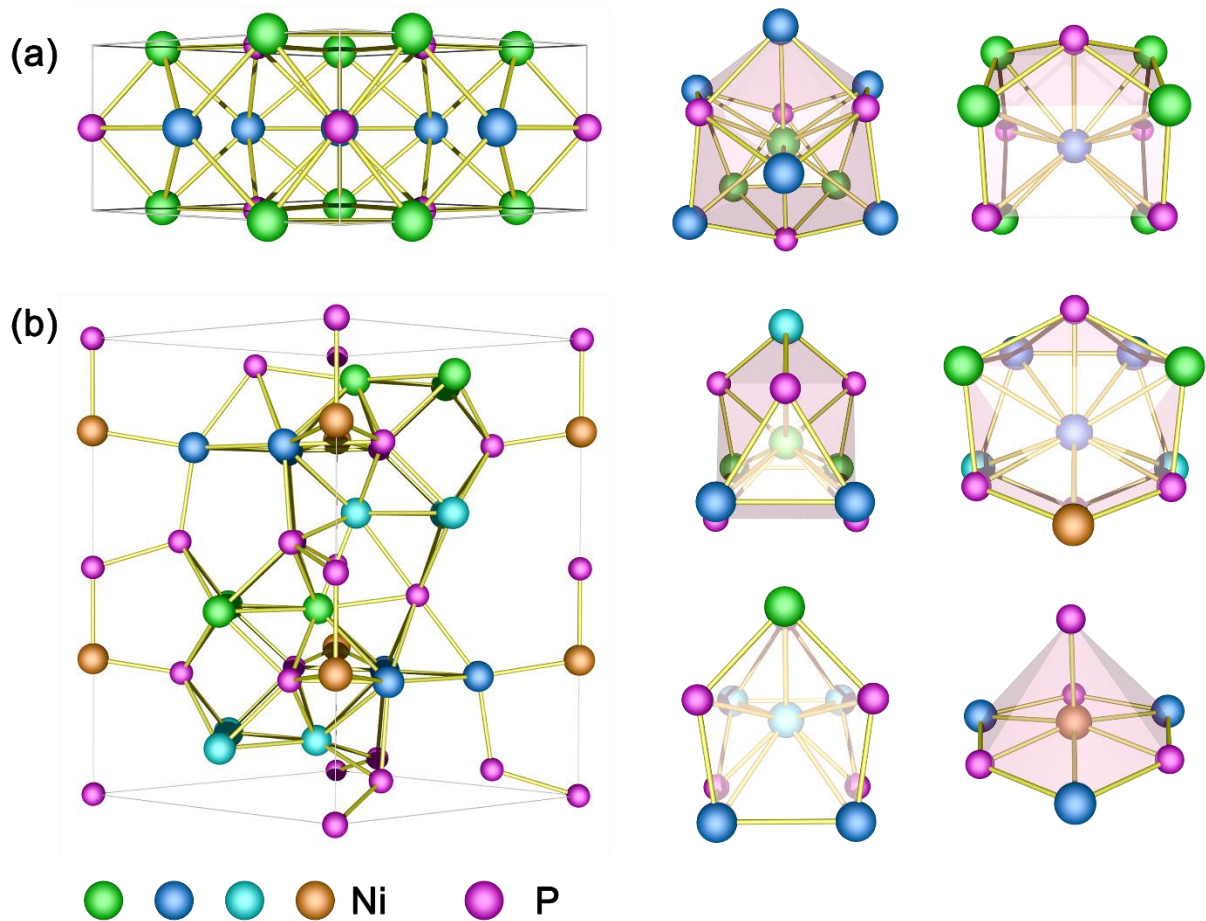


Fig. S3. The crystal structure (left panel) and coordination environment of Ni (right panel) of (a) Ni_2P and (b) Ni_3P_4 . Considering the very close ionic radius, the coordination environment of Fe can be the same as that of Ni.

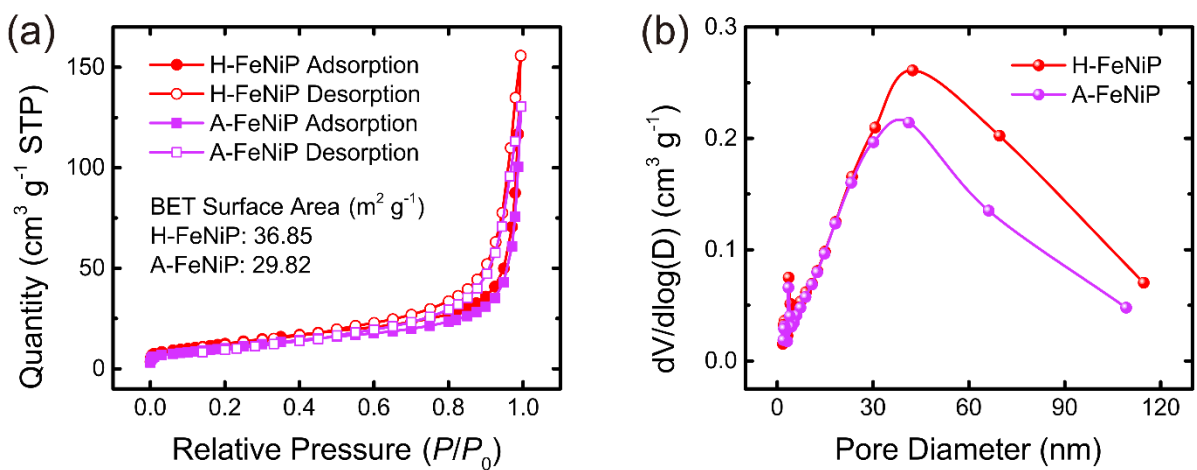


Fig. S4. (a) The isothermal N_2 adsorption-desorption and (b) pore distribution curves of A-FeNiP and H-FeNiP.

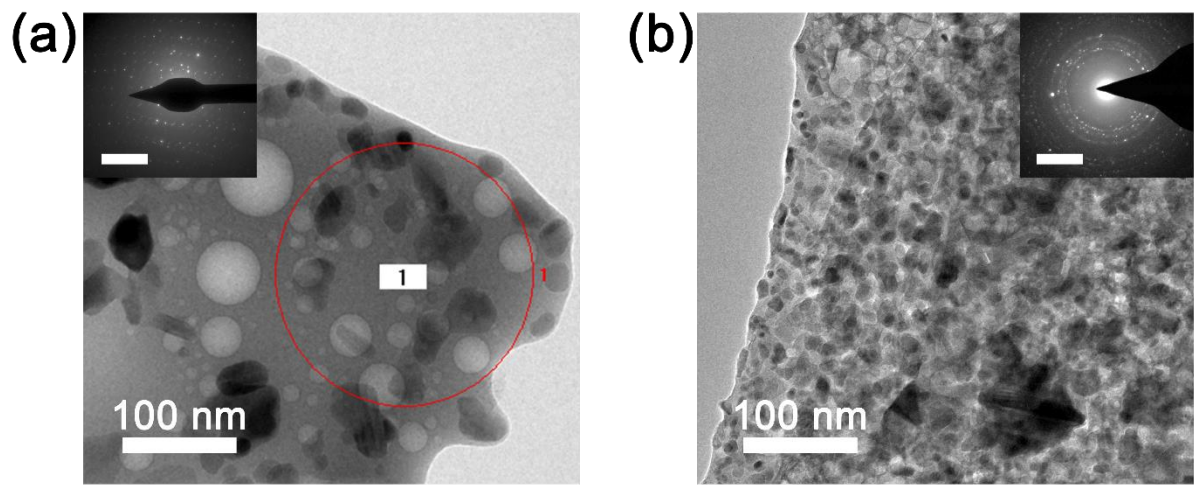


Fig. S5. The TEM and SAED images of (a) A-FeNiP and (b) H-FeNiP. The scale bars of insert are 5 nm^{-1} .

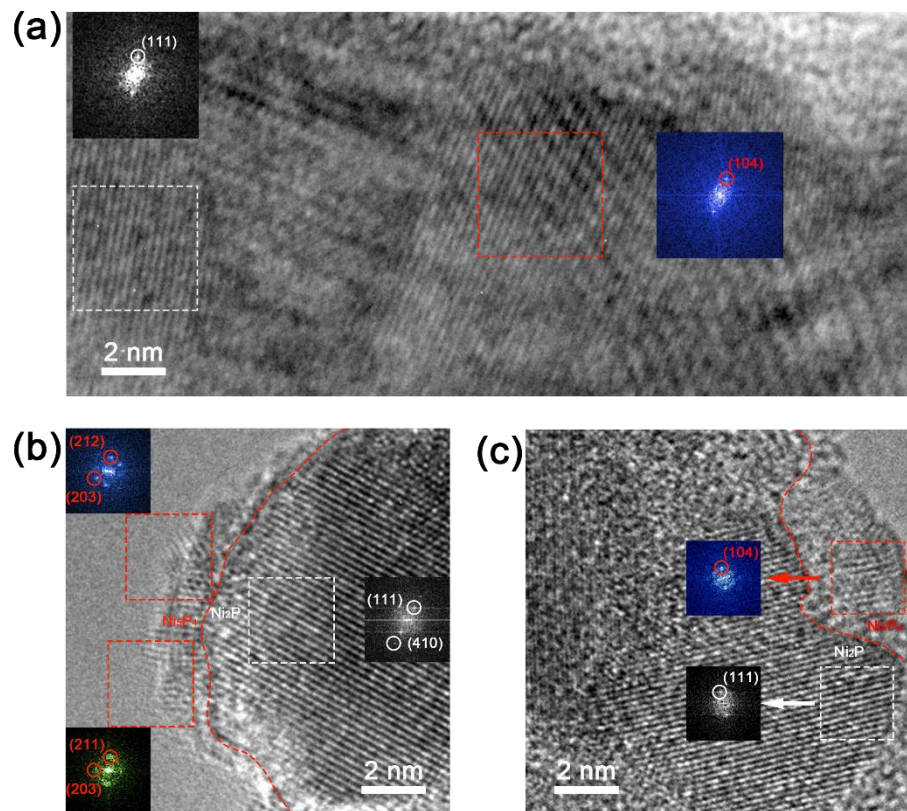


Fig. S6. HRTEM images and the corresponding FFT patterns of (a) A-FeNiP, and (b, c) two individual areas of H-FeNiP.

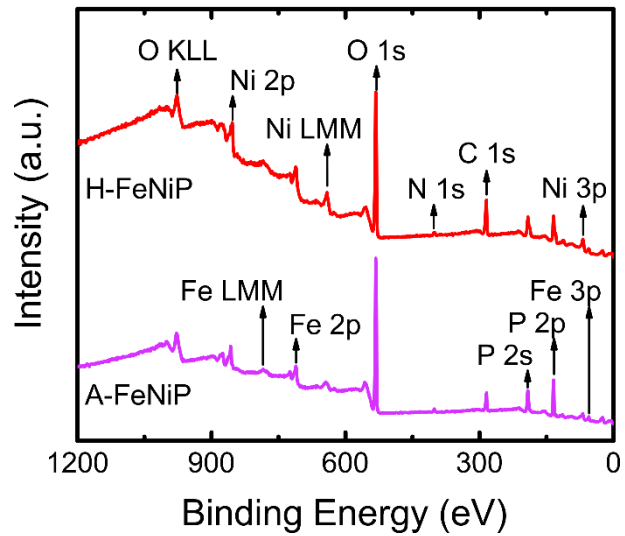


Fig. S7. XPS survey spectra of A-FeNiP and H-FeNiP.

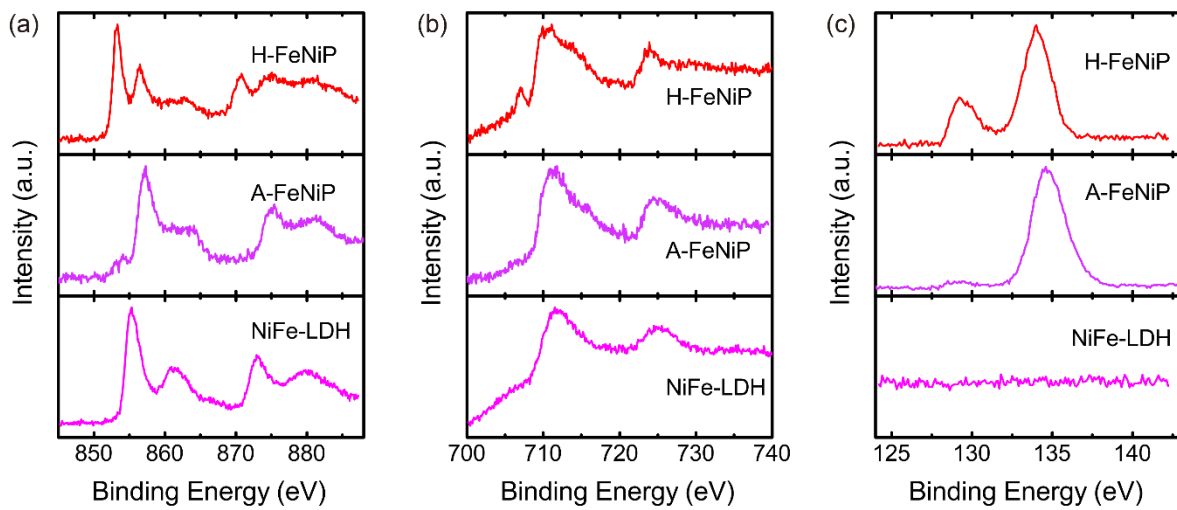


Fig. S8. High-resolution XPS spectra of (a) Ni 2p, (b) Fe 2p and (c) P 2p.

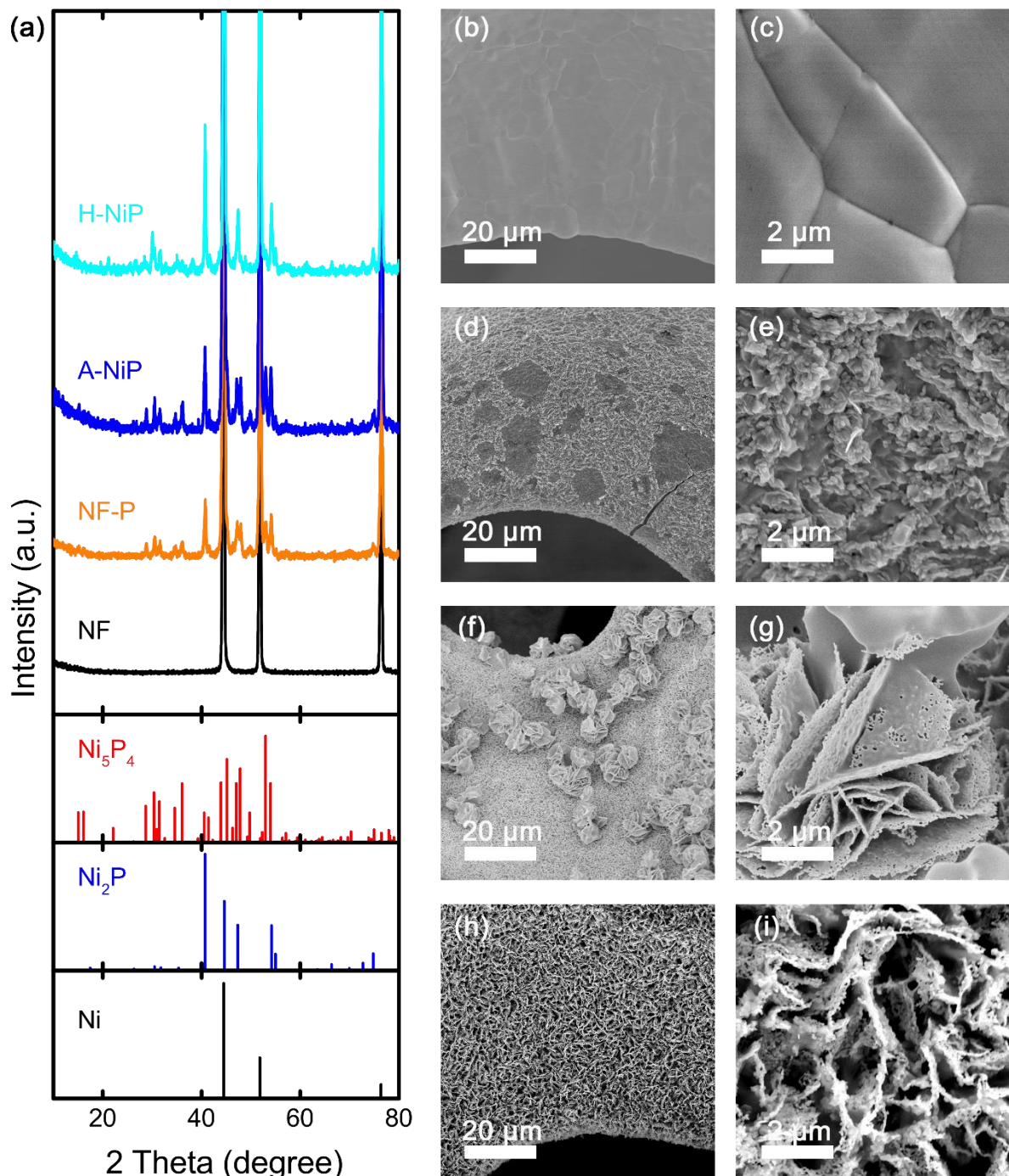


Fig. S9. (a) XRD patterns and the standard diffraction patterns of Ni_5P_4 , Ni_2P and Ni. SEM images of (b, c) NF, (d, e) NF-P, (f, g) A-NiP and (h, i) H-NiP.

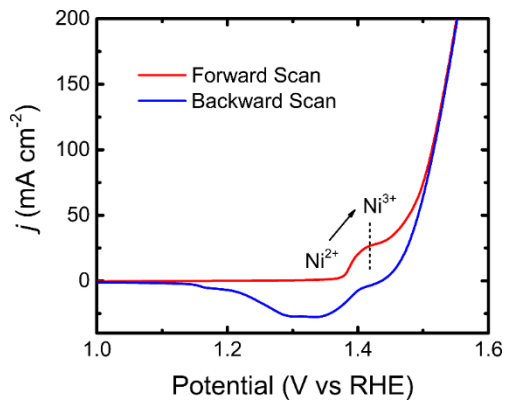


Fig. S10. The forward and backward OER scan curves of H-FeNiP.

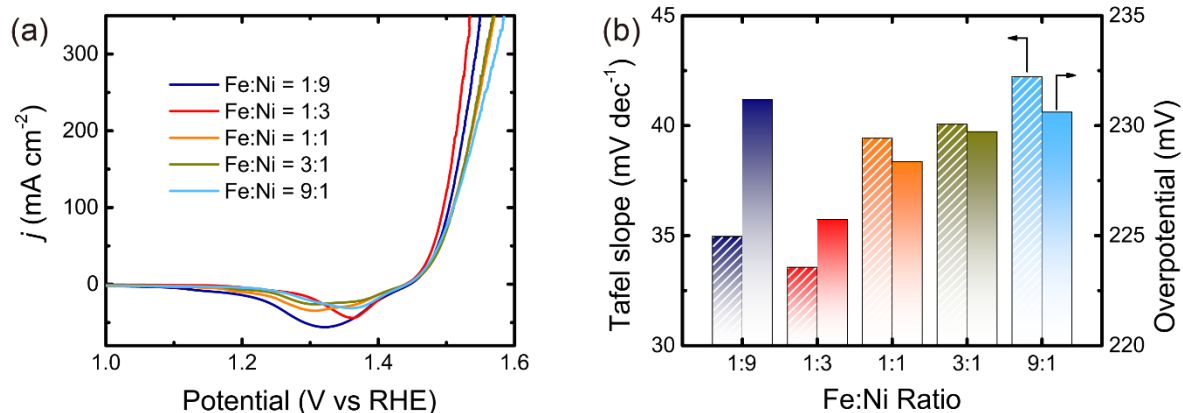


Fig. S11. Influence of Ni:Fe ratio on OER performance. (a) Anodic polarization curves and (b) summary of Tafel slope and η_{10} .

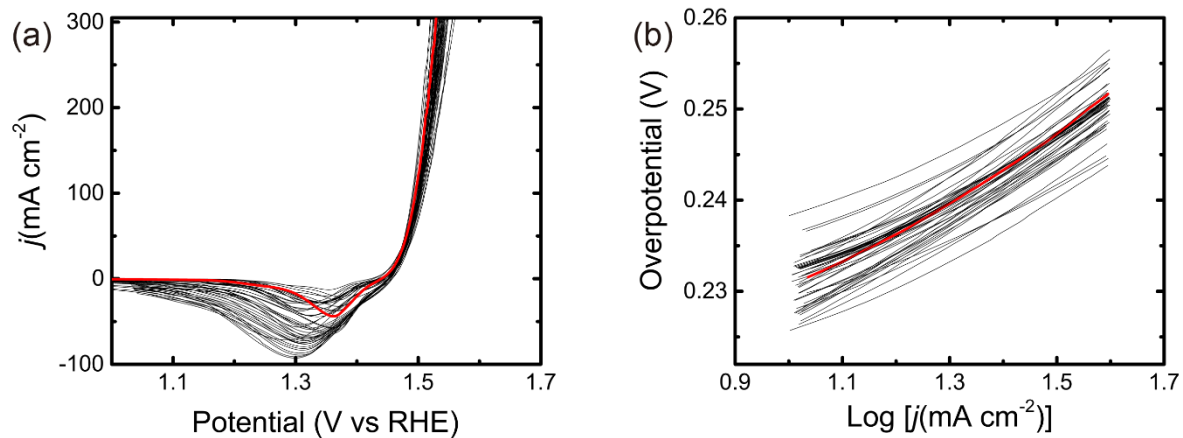


Fig. S12. Statistical studies on OER performance of H-FeNiP. (a) Polarization curves and (b) Tafel plots.

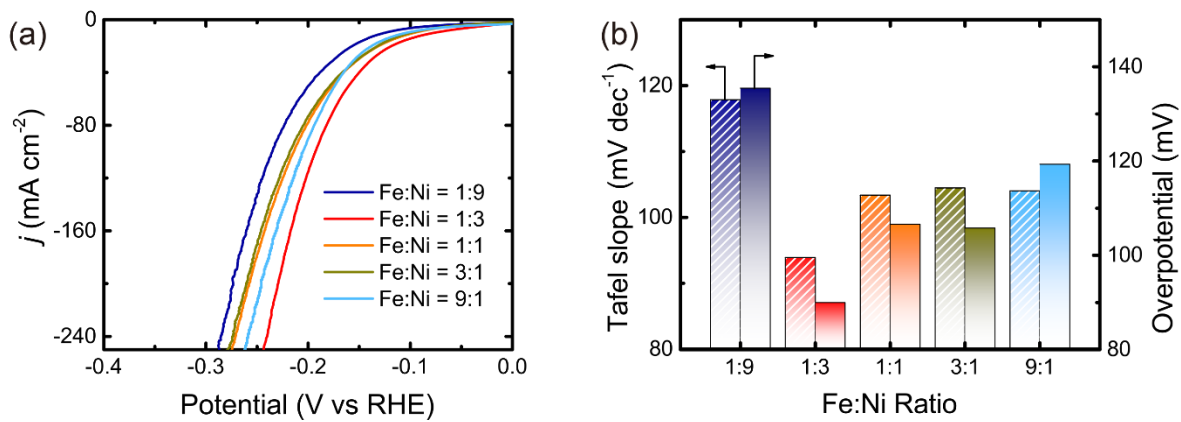


Fig. S13. Influence of Ni:Fe ratio on HER performance. (a) Cathodic polarization curves and (b) summary of Tafel slope and η_{10} .

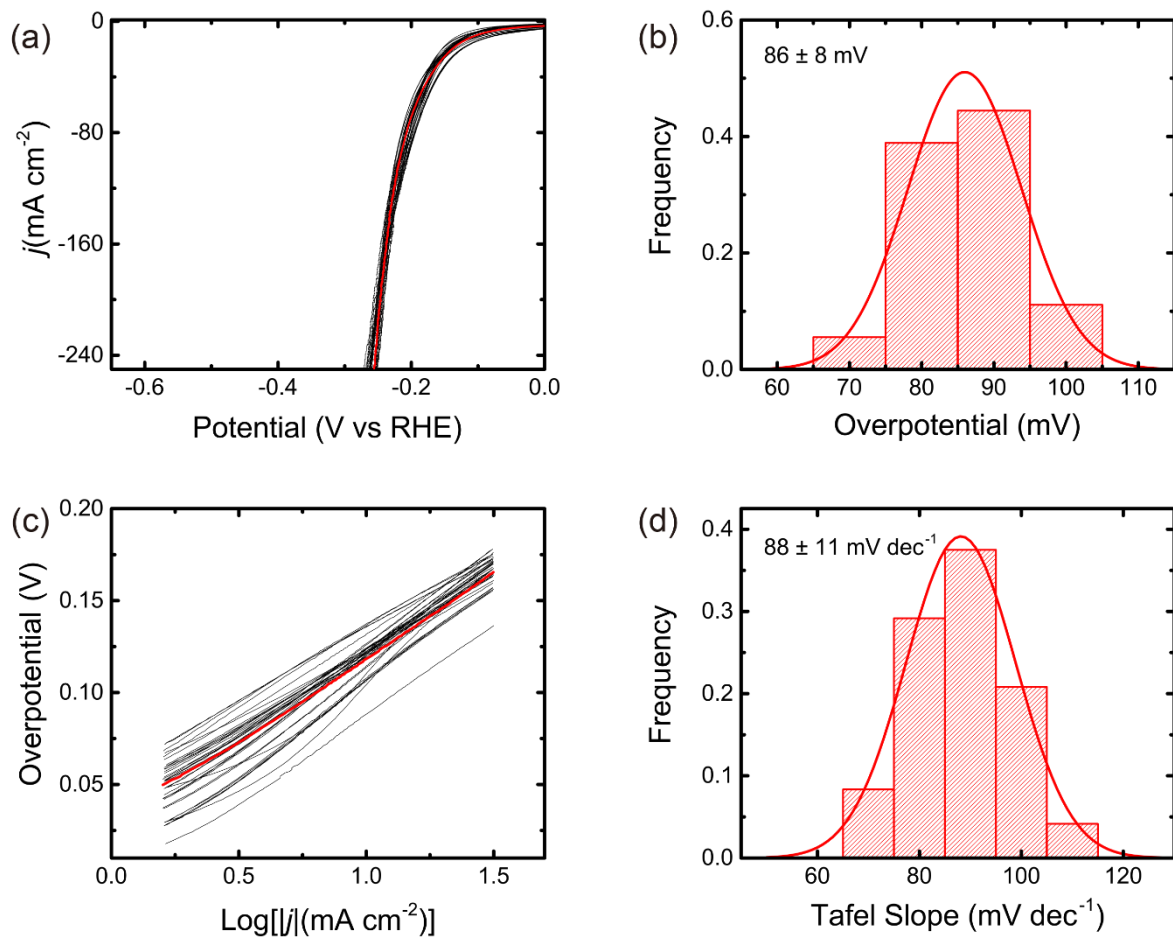


Fig. S14. Statistical studies on HER performance of H-FeNiP. (a) Polarization curves. (b) Statistics on η_{10} . (c) Tafel plots. (d) Statistics on Tafel slopes.

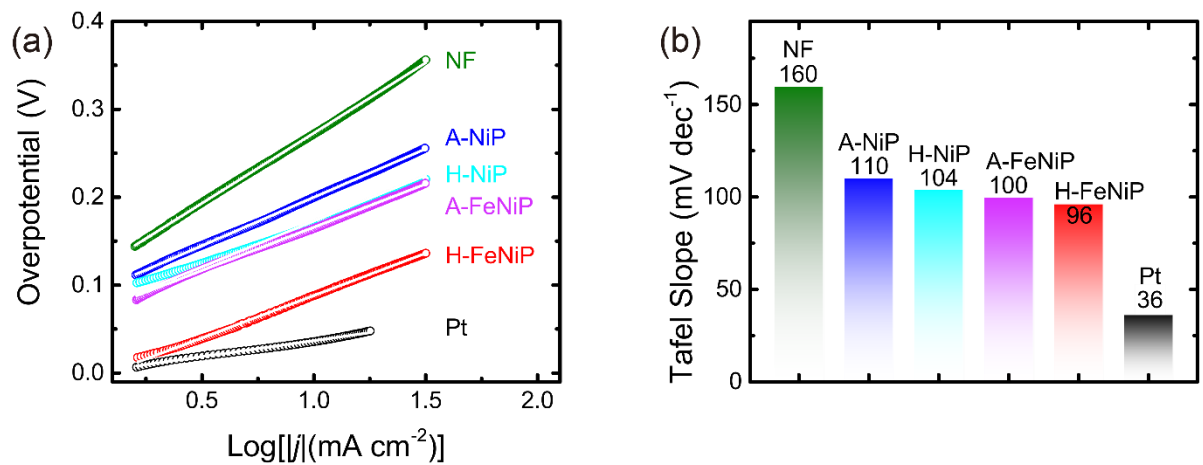


Fig. S15. (a) Tafel plots for HER and (b) the corresponding Tafel slopes.

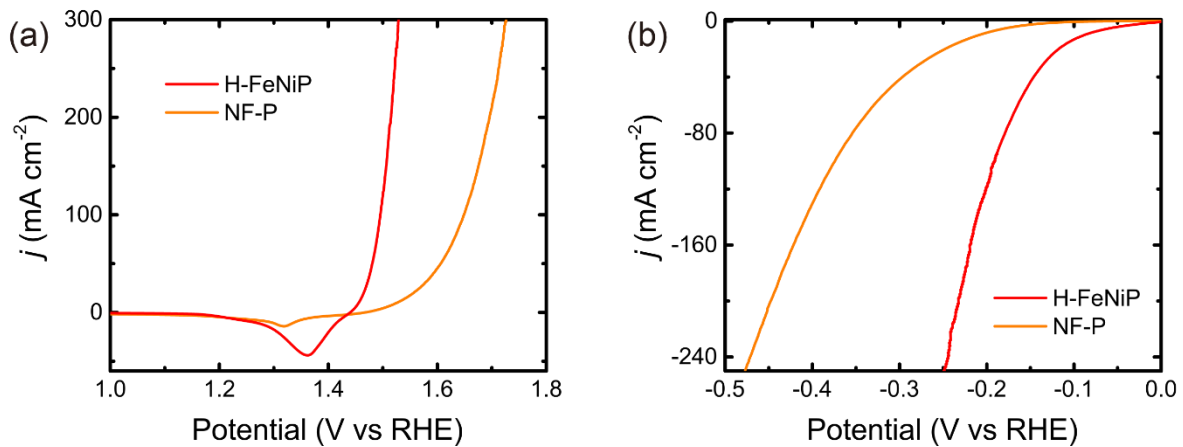


Fig. S16. The electrocatalytic activity of H-FeNiP in comparison with NF-P. (a) OER and (b) HER.

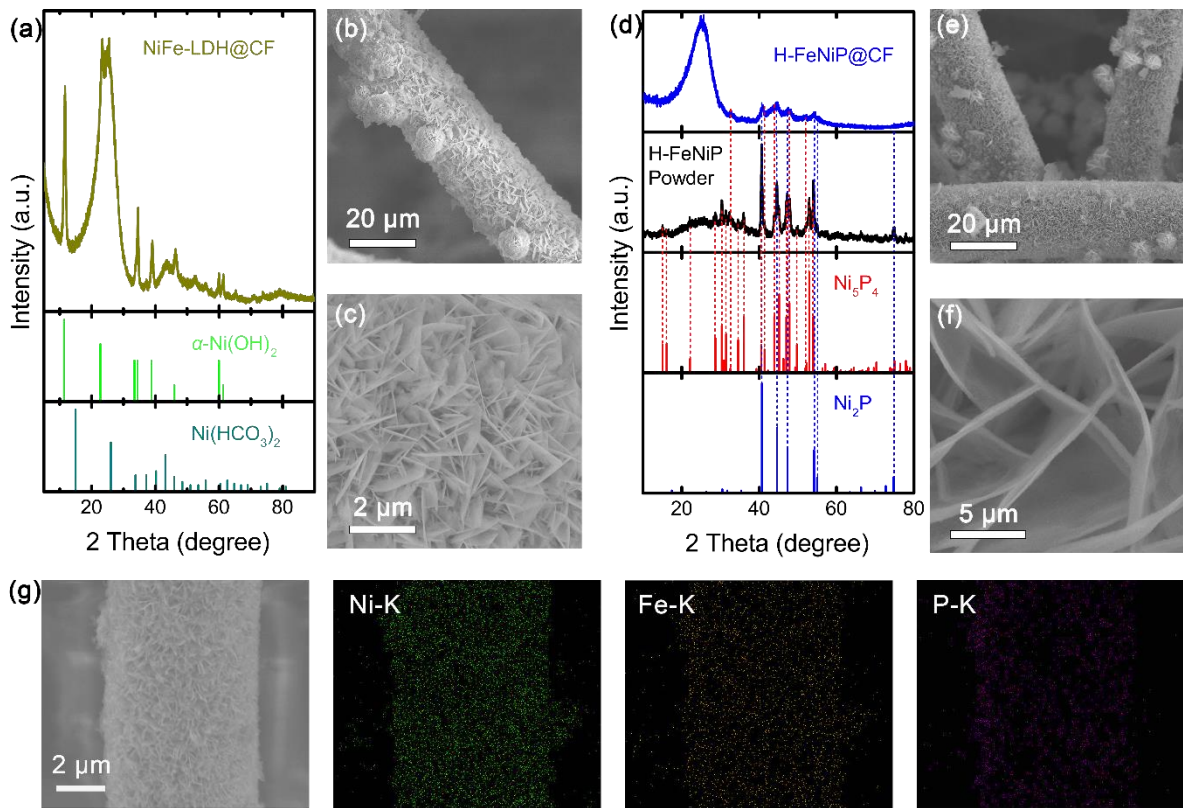


Fig. S17. (a) The XRD pattern and (b, c) SEM images of NiFe-LDH@CF. (d) The XRD pattern and (e, f) SEM images of H-FeNiP@CF. (g) SEM elemental mapping images of P, Fe and Ni for H-FeNiP@CF.

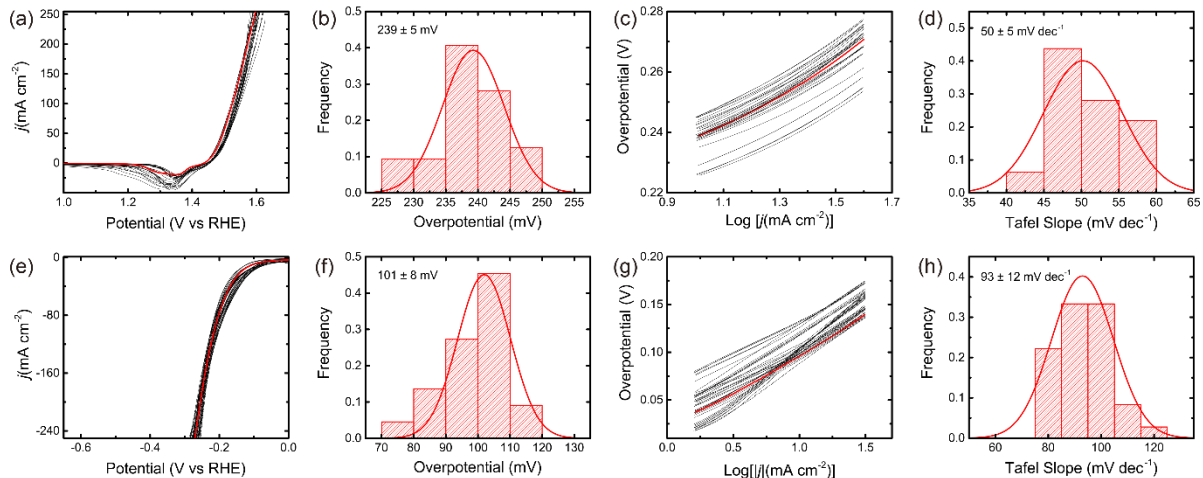


Fig. S18. Statistical studies on electrocatalytic performance of H-FeNiP@CF. (a) Polarization curves, (b) statistics on η_{10} , (c) Tafel plots and (d) statistics on Tafel slopes for OER. (e) Polarization curves, (f) statistics on η_{10} , (g) Tafel plots and (h) statistics on Tafel slopes for HER.

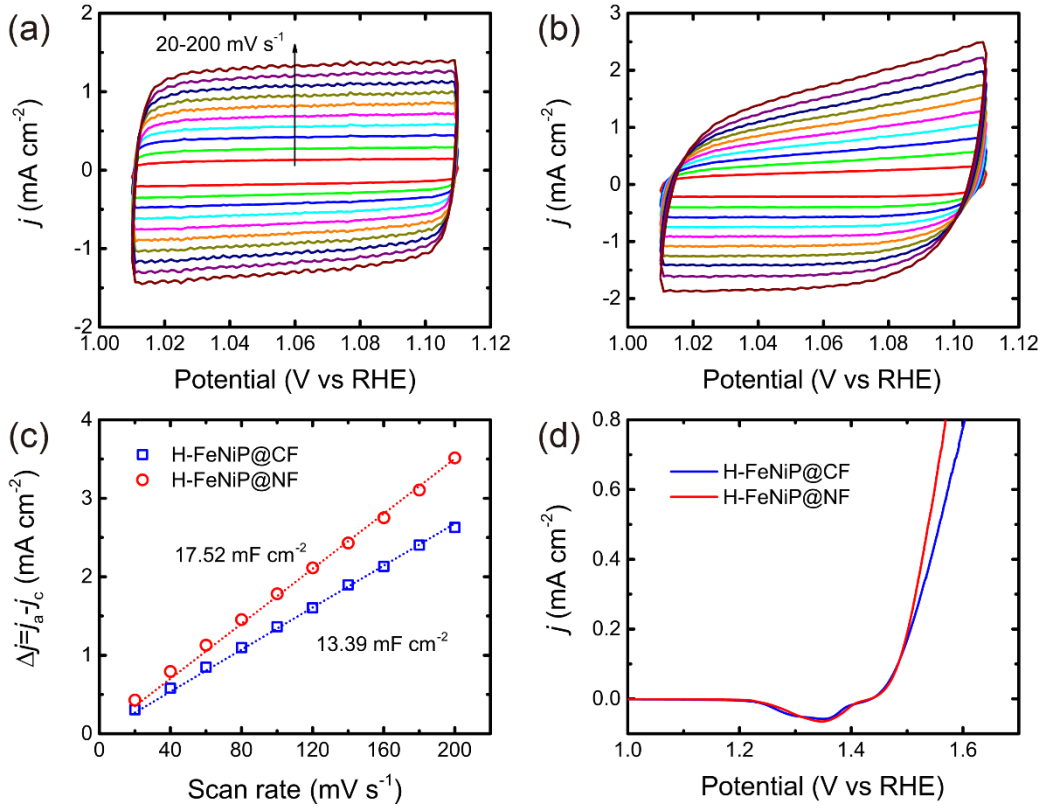


Fig. S19. Measurements of the double-layer capacitance (C_{dl}) in the anodic region. CV curves for (a) H-FeNiP@CF and (b) H-FeNiP@NF from 20 to 200 mV s⁻¹ with an interval of 20 mV s⁻¹. (c) The differences in current density variation ($\Delta j = j_a - j_c$) at the potential of 1.06 V vs RHE as a function of scan rates. To estimate the ECSA, a factor of 40 μ F cm⁻² per cm² ECSA is used in calculations, yielding 334.75 cm⁻² for H-FeNiP@CF and 438.00 cm⁻² for H-FeNiP@NF, respectively. (d) Polarization curves for OER normalized by ECSA.

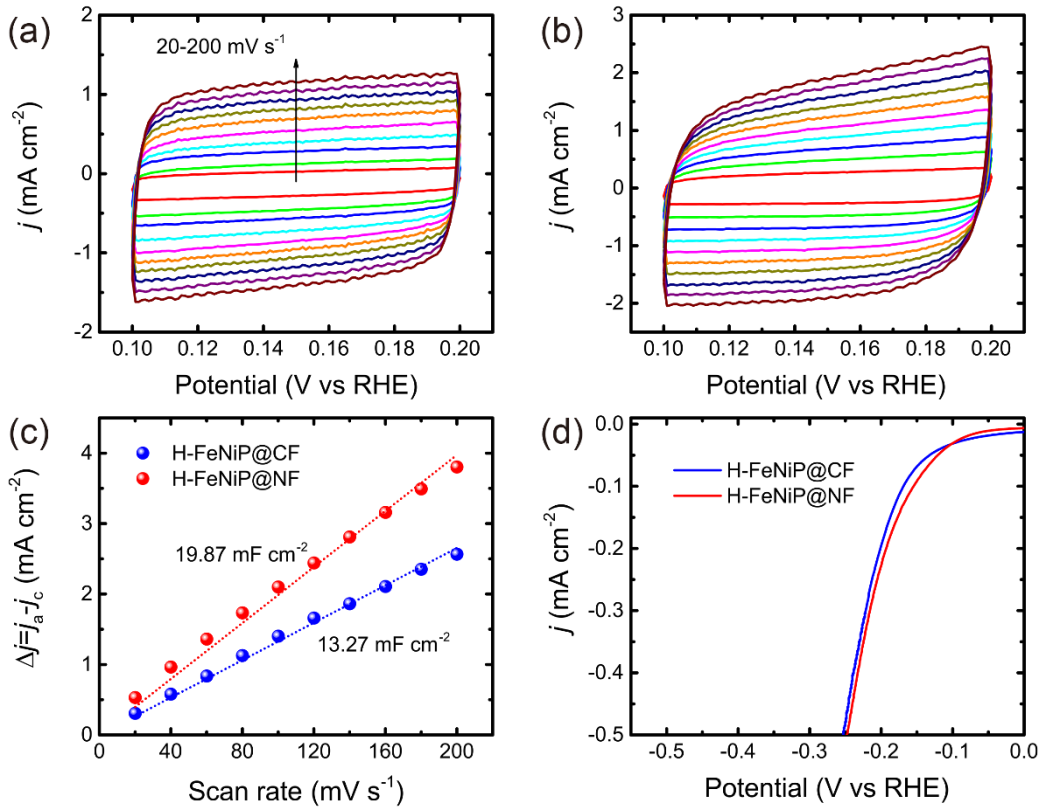


Fig. S20. Measurements of the double-layer capacitance (C_{dl}) in the cathodic region. CV curves for (a) H-FeNiP@CF and (b) H-FeNiP@NF from 20 to 200 mV s⁻¹ with an interval of 20 mV s⁻¹. (c) The differences in current density variation ($\Delta j = j_a - j_c$) at the potential of 0.15 V vs RHE as a function of scan rates. The ECSA is estimated to be 331.75 cm⁻² for H-FeNiP@CF and 496.75 cm⁻² for H-FeNiP@NF, respectively. (d) Polarization curves for HER normalized by ECSA.

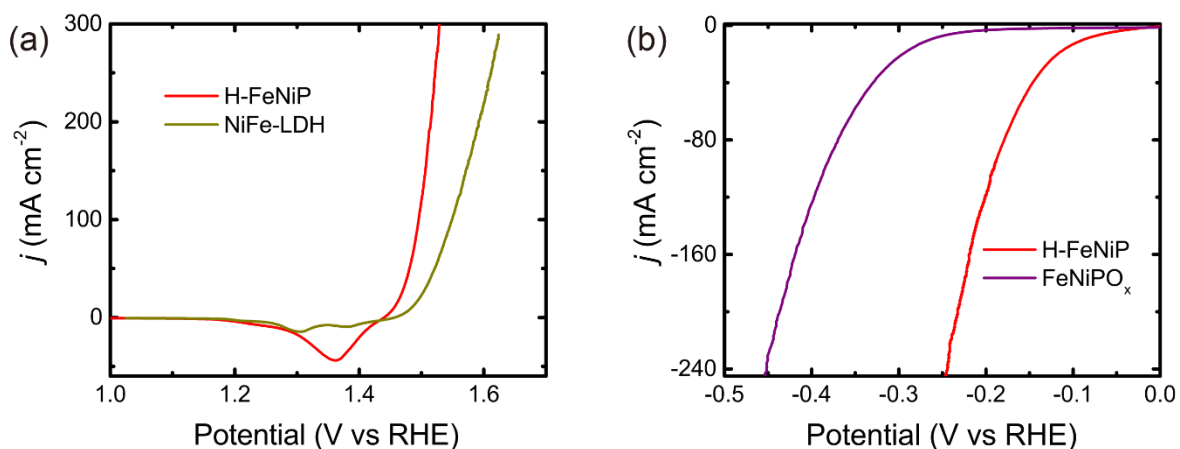


Fig. S21. (a) The OER activity of H-FeNiP vs NiFe-LDH. (b) The HER activity of H-FeNiP vs H-FeNiPO_x.

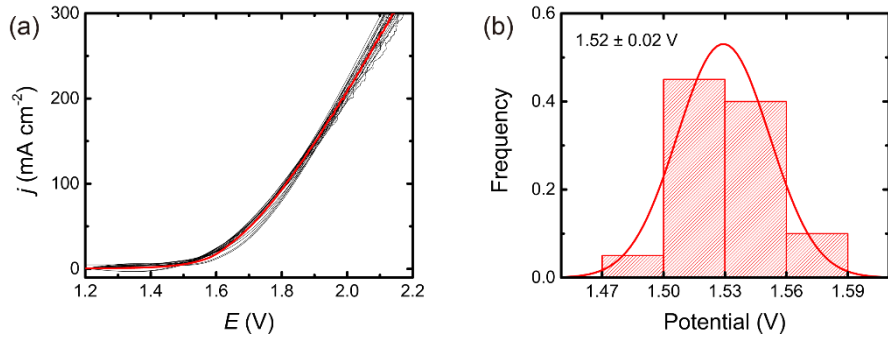


Fig. S22. Statistical studies on the overall water splitting performances of H-FeNiP. (a) Polarization curves in two-electrode system. (b) Statistics on cell potentials for the current density of 10 mA cm^{-2} .

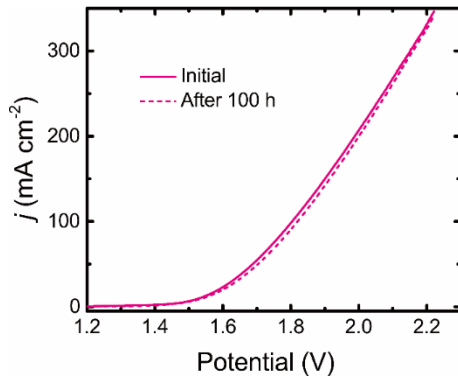


Fig. S23. Polarization curves of the H-FeNiP couple before and after stability test.

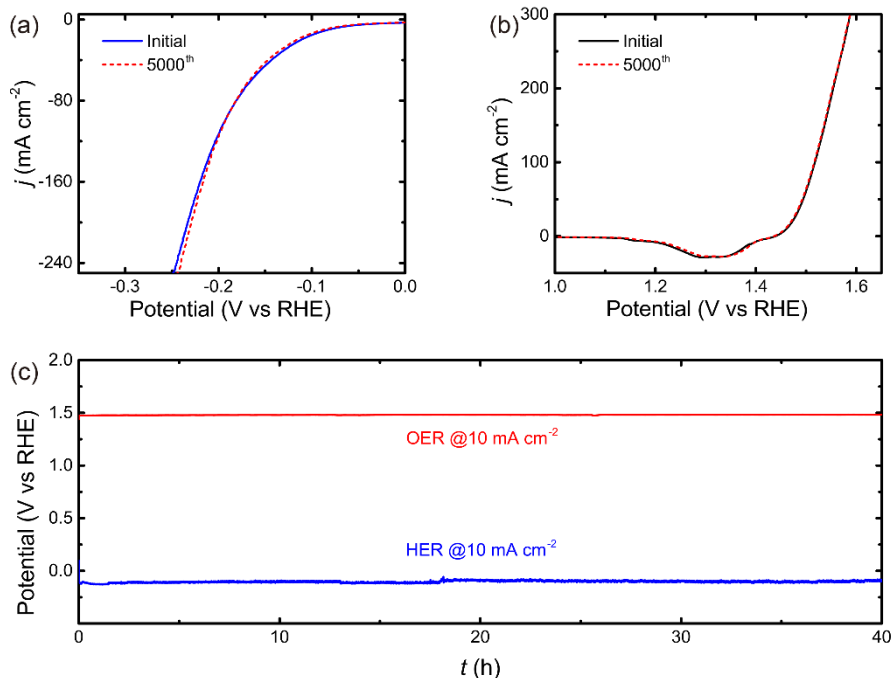


Fig. S24. Stability and durability tests of H-FeNiP. Polarization curves for (a) HER and (b) OER before and after 5000 continuous CV cycles. Scan rate: 100 mV s^{-1} . Scan region: $-0.2\text{--}0.2 \text{ V vs RHE}$ for HER and $1.2\text{--}1.6 \text{ V vs RHE}$ for OER. (c) Chronopotentiometry curves for HER and OER at the current density of 10 mA cm^{-2} .

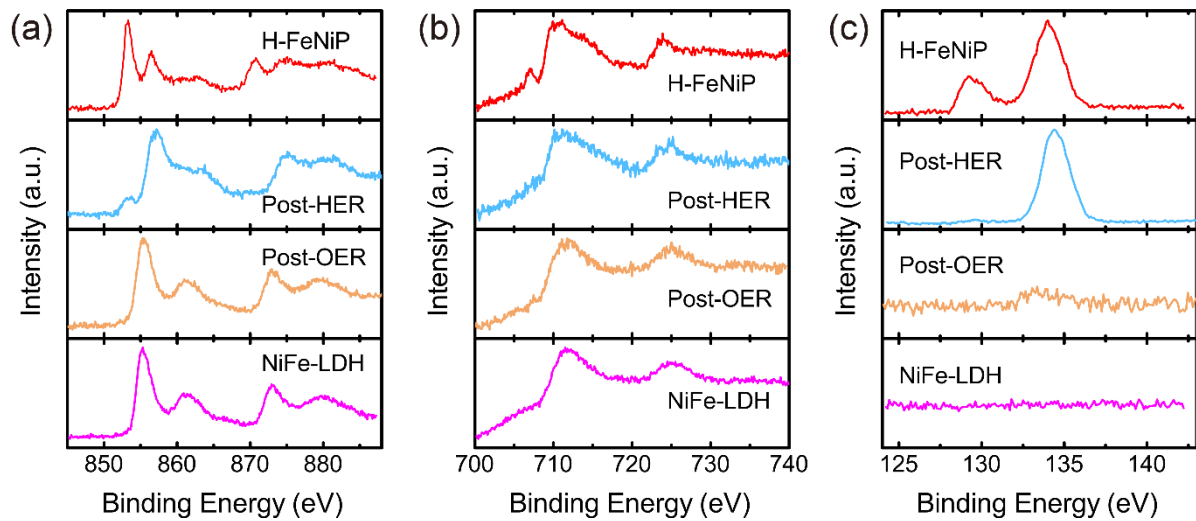


Fig. S25. High-resolution XPS spectra of (a) Ni 2p, (b) Fe 2p and (c) P 2p. It can be seen that the spectra of Post-OER are resemble to those of NiFe-LDH, indicating surface transition during OER. Although the intensity of M-P related peaks suffer decrease, the spectra of Post-HER are still close to those of H-FeNiP, indicating the preservation of surface species.

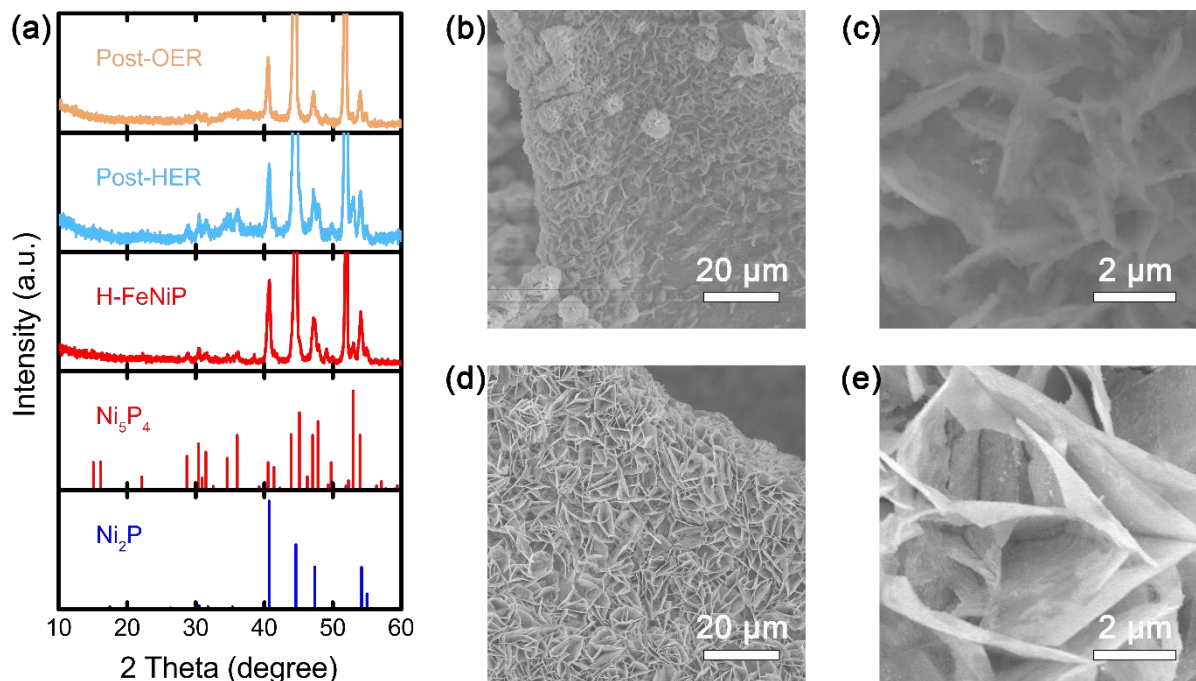


Fig. S26. Characterizations of H-FeNiP after stability tests. (a) XRD patterns. SEM images of (b, c) post-OER and (d, e) post-HER samples.

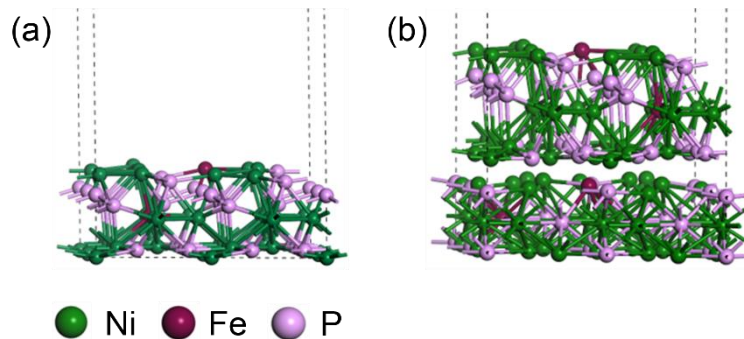


Fig. S27. The structure of (a) Fe-Ni₅P₄ for A-FeNiP and (b) Fe-Ni₅P₄/Fe-Ni₂P for H-FeNiP.

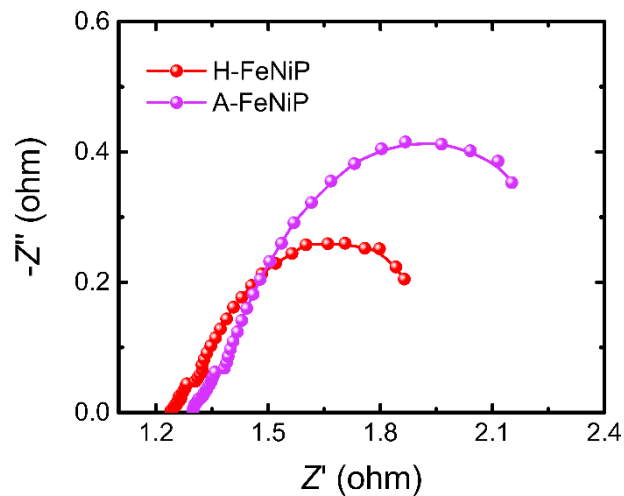


Fig. S28. Electrochemical impedance spectroscopy of A-FeNiP and H-FeNiP at an overpotential of 200 mV for HER.

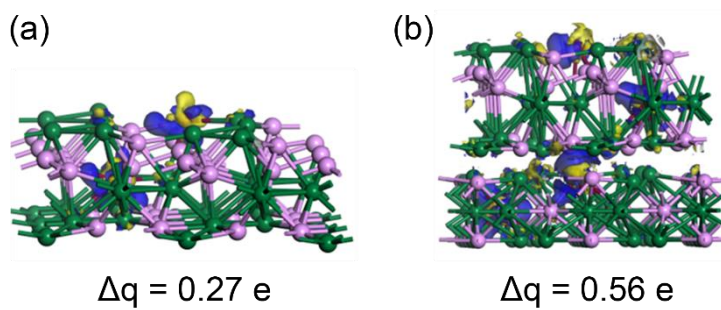


Fig. S29. Differential charge density of (a) Fe-Ni₅P₄ and (b) Fe-Ni₅P₄/Fe-Ni₂P. The yellow color represents the charge depletion and the blue color represents the charge accumulation in the space. Δq is the charge transfer quantity.

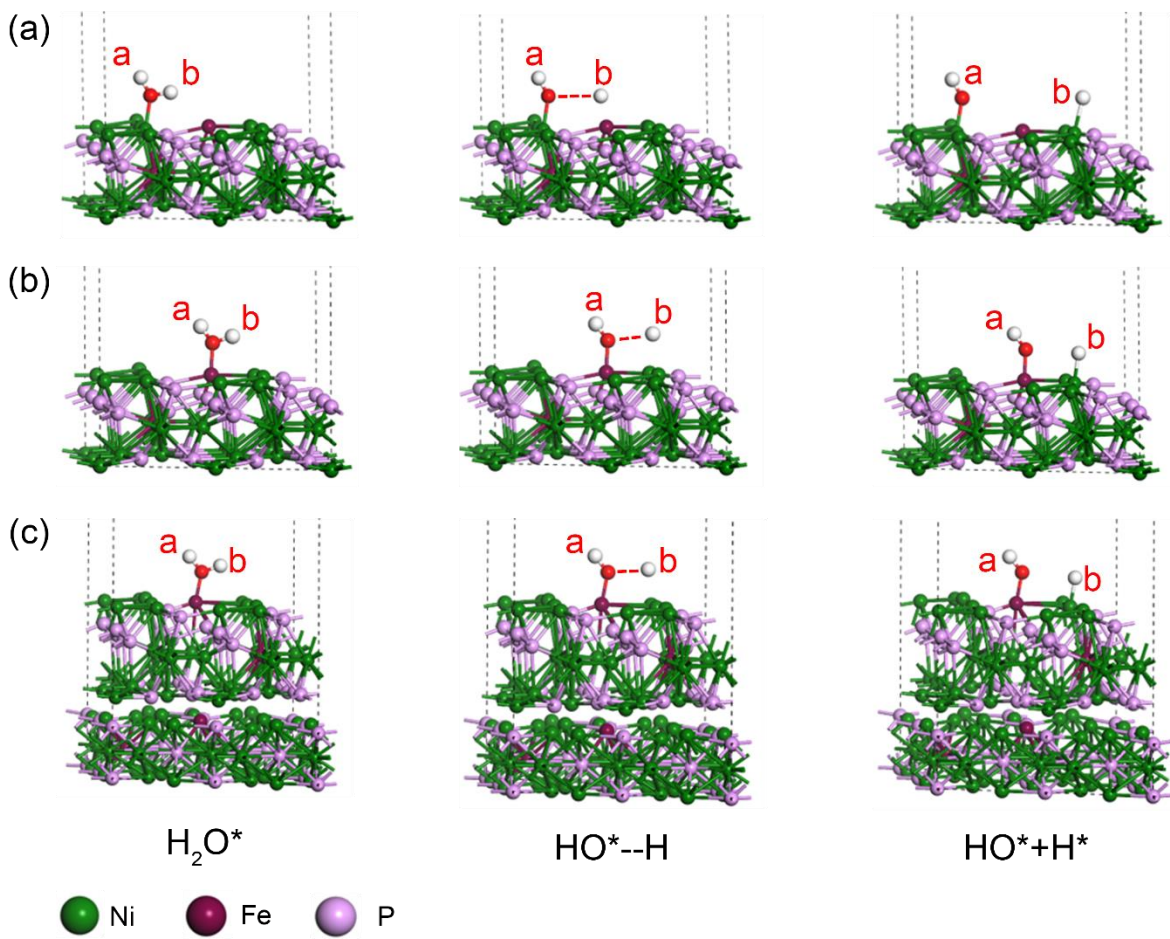


Fig. S30. H_2O dissociation processes on (a) the Ni site of A-FeNiP, (b) the Fe site of A-FeNiP and (c) the Fe site of H-FeNiP. The bonds distances are shown in Table S4.

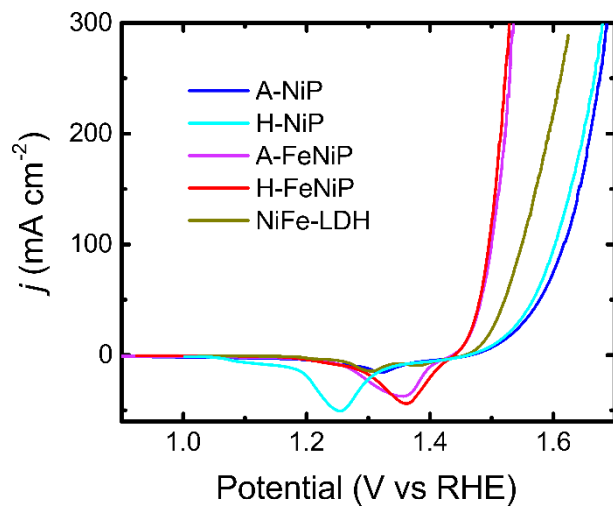


Fig. S31. OER activity trend within H-FeNiP, A-FeNiP, NiFe-LDH, A-NiP and H-NiP.

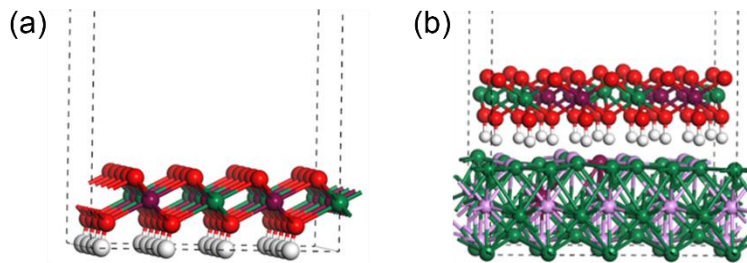


Fig. S32. The structure diagrams of (a) NiFe-LDH and (b) NiFe-LDH/Fe-Ni₂P. The Ni, Fe, P, O and H atoms are represented by olive, wine, pink, red and white spheres, respectively.

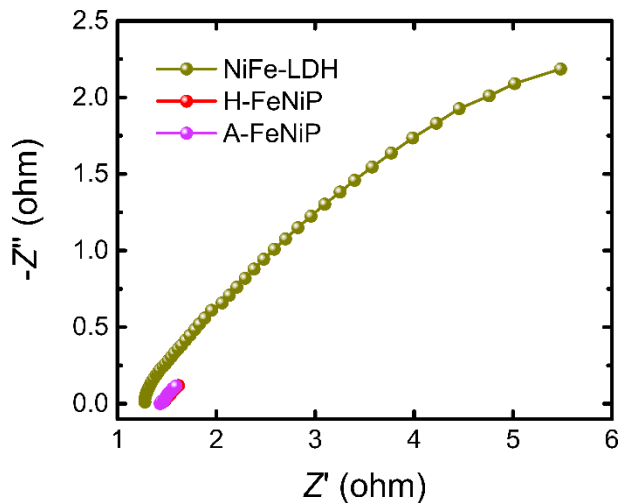


Fig. S33. Electrochemical impedance spectroscopy of NiFe-LDH, A-FeNiP and H-FeNiP at an overpotential of 270 mV for OER.

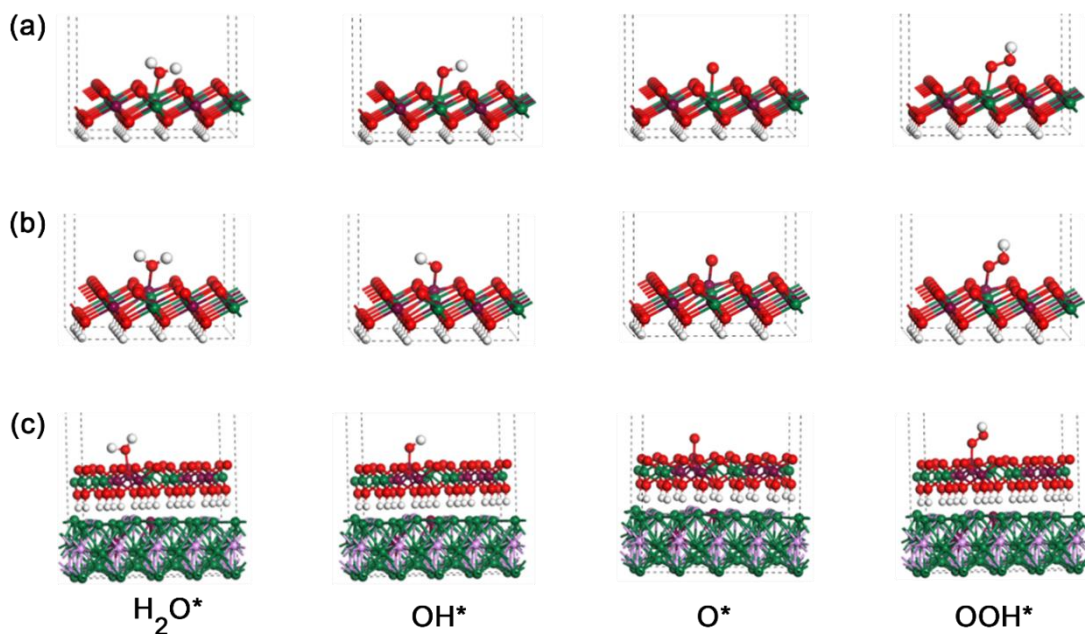


Fig. S34. Optimized configuration of OER intermediates on (a) the Ni site of NiFe-LDH, (b) the Fe site of NiFe-LDH and (c) the Fe site of NiFe-LDH/Fe-Ni₂P.

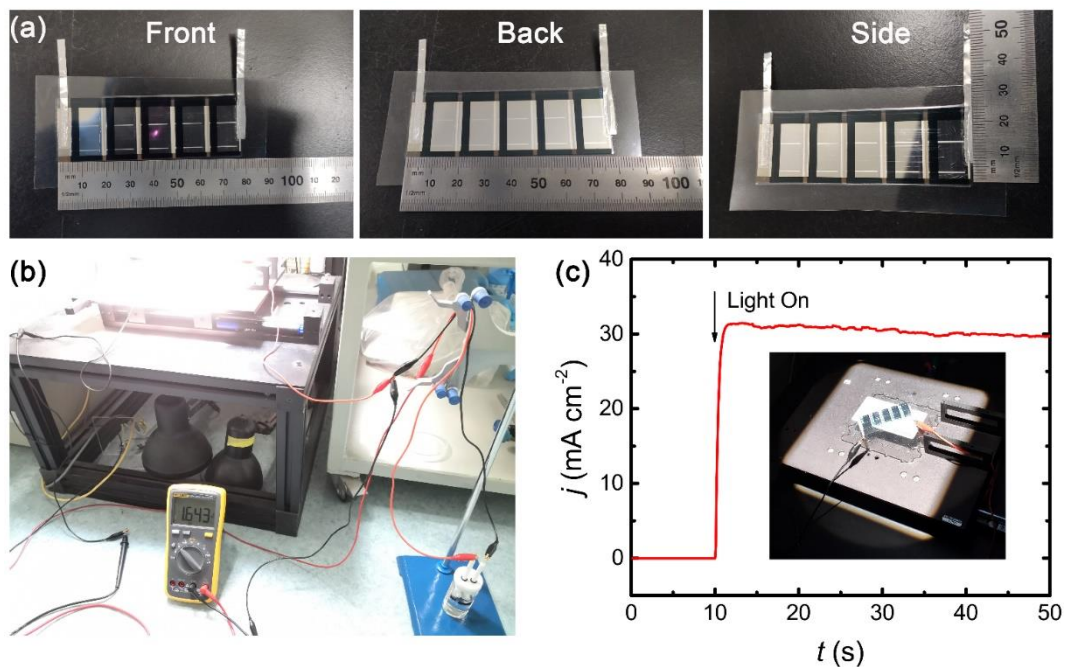


Fig. S35. (a) Photographs of the PTB7-Th/PC₇₁BM/CO_I8DFIC solar cell. (b) Photograph of the solar-driven water-splitting experiment. The electrolytic cell and the electrochemistry workstation are in series with the OSC. (c) J - t curve of the developed STH system. The insert picture shows the facula and the OSC.

Table S1. Comparison of the OER performance of the latest reported highly active nanoarray electrocatalysts in 1 M KOH.

Catalysts	η_{10} (mV)	Tadel slope (mV dec ⁻¹)	Ref.
H-FeNiP	231 ± 3	32 ± 4	This work
Ni _{1.5} Fe _{0.5} P/CF	264	55	1
NiFe/NiFe:Pi	290	38	2
np-(Ni _{0.67} Fe _{0.33}) ₄ P ₅	245	32.9	3
(NiFe)PS ₃	275	41.7	4
Ni ₃ FeN/r-GO-20	270	54	5
DR-Ni ₃ FeN/N-G	250	38	6
Fe-Ni ₃ S ₂ /FeNi	282	54	7
Fe-NiSe ₂ UNWs	268	41	8
Ni-Fe LDH hollow nanoprisms	280	49.4	9
a-LNF(t-d)	249	36	10
HG-NiFe	310	39	11
hcp-FeNi@NC	226	41	12
TA-Ni ₃ Fe	290	28	13
NiFe@NFF	227	38.9	14
Co-P film	345	47	15
Ni ₅ P ₄	290	40	16
CoP-MNA	290	65	17
CoFePO	274.5	51.7	18
CP@Ni-P	190	73	19
NiCo ₂ S ₄ NW/NF	260	40.1	20
Ni _{0.51} Co _{0.49} P	239	45	21
porous MoO ₂ /Ni foam	260	54	22
np-(Co _{0.52} Fe _{0.48}) ₂ P	270	30	23
NiCoP/NF	280	87	24
VOOH	270	68	25
Fe-CoP/Ti	230	67	26
Cu@NiFe LDH	199	27.8	27
NiFe LDH@NiCoP/NF	220	48.6	28
NiFeRu-LDH	225	32.4	29
Ni ₁₁ (HPO ₃) ₈ (OH) ₆ /NF	232	91	30

Table S2. Comparison of the HER performance of the latest reported highly active nanoarray electrocatalysts in 1 M KOH.

Catalysts	η_{10} (mV)	Tadel slope (mV dec ⁻¹)	Ref.
H-FeNiP	86 ± 8	100 ± 7	This work
(Ni _{0.33} Fe _{0.67}) ₂ P	84	73.2	31
Ni-doped FeP/C	95	72	32
Ni-Fe-P/NF	98	50	33
(Fe _x Ni _{1-x}) ₂ P	103	41.6	34
Ni _{1.85} Fe _{0.15} P NSAs/NF	106	89.7	35
NiFeP/NM	111	83.9	36
Ni ₂ P/Fe ₂ P	121	67	37
NiP/NiFeP/C	138	68	38
Ni _{1.5} Fe _{0.5} P/CF	158	125	1
Ni/NiP	130	58.5	39
Ni ₅ P ₄	150	53	16
h-NiS _x	60	99	40
CP@Ni-P	117	85.4	19
MoO _x /Ni ₃ S ₂ /NF	106	90	41
np-(Co _{0.52} Fe _{0.48}) ₂ P	79	40	23
VOOH	164	104	25
Fe-CoP/Ti	78	75	26
Cu@NiFe LDH	116	58.9	27
NiFe LDH@NiCoP/NF	120	88.2	28
Se-(NiCo)S/OH	101	87.3	42
Ni ₁₁ (HPO ₃) ₈ (OH) ₆ /NF	121	102	30
Ni ₂ P@NPCNFs	104.2	79.7	43
CoP/NiCoP	133	88	44
p-FGDY/CC	82	139	45
NCP-3	78	173	46
CoP/NPC/TF	80	50	47
CoFeZr oxides /NF	104	119.3	48
MoC-Mo ₂ C/PNCDs	121	60	49
CoP/NiCoP/NC	75	59	50
Al-CoS ₂	86	62.47	51

TableS3. Summary of overall water splitting performance of the latest reported highly active bifunctional nanoarray electrocatalysts.

Catalysts	E_{10} (V)	Ref.
H-FeNiP	1.53 ± 0.02	This work
CoP-MNA	1.62	17
CoFePO	1.56	18
CP@Ni-P	1.63	19
Ni/NiP	1.61	39
NiCo ₂ S ₄ NW/NF	1.63	20
np-(Co _{0.52} Fe _{0.48}) ₂ P	1.53	23
NiCoP/NF	1.58	24
VOOH	1.62	25
Co ₃ O ₄ -MTA	1.63	52
Fe-CoP/Ti	1.6	26
Cu@CoS _x /CF	1.5	53
Cu@NiFe LDH	1.54	27
Co ₁ Mn ₁ CH	1.68	54
N-NiMoO ₄ /NiS ₂	1.6	55
CoP/NCNHP	1.64	56
NiFe LDH@NiCoP/NF	1.57	28
Se-(NiCo)S/OH	1.6	42
Ni–Co–P HNBs	1.64	57
Ni ₁₁ (HPO ₃) ₈ (OH) ₆ /NF	1.6	30
Co-NC@Mo ₂ C	1.685	58
Co/β-Mo ₂ C@N-CNTs	1.64	59
Co/CNFs (1000)	1.69	60
Co ₃ S ₄ /EC-MOF	1.55	61
NiCo ₂ S ₄ -4	1.58	62
NOGB-800	1.65	63
Co@N-CS/N-HCP@CC	1.545	64
Cu ₃ N/NF	1.60 ± 0.01	65
MoS ₂ /LDH	1.57	66
MoS ₂ /Co ₉ S ₈ /Ni ₃ S ₂ /Ni	1.54	67
CoFeZr oxides /NF	1.63	48

Table S4. Bond distance for the intermediates of HER (Å).

		H ₂ O*		HO*--H		HO*+H*	
H-FeNiP	Ni site	H-O ^a	1.256	H-O ^a	1.340	H-O ^a	1.204
		H-O ^b	1.279	H-O ^b	2.866	Ni-H ^b	2.082
		Ni-O	1.817	Ni-O	1.992	Ni-O	1.861
	Fe site	H-O ^a	1.211	H-O ^a	1.226	H-O ^a	1.266
		H-O ^b	1.224	H-O ^b	2.502	Ni-H ^b	1.925
		Fe-O	2.026	Fe-O	2.177	Fe-O	1.807
A-FeNiP	Ni site	H-O ^a	1.128	H-O ^a	1.212	H-O ^a	1.204
		H-O ^b	1.125	H-O ^b	2.447	Ni-H ^b	2.271
		Ni-O	2.207	Ni-O	2.309	Ni-O	2.124
	Fe site	H-O ^a	1.201	H-O ^a	1.258	H-O ^a	1.329
		H-O ^b	1.219	H-O ^b	2.390	Ni-H ^b	2.160
		Fe-O	2.257	Fe-O	2.252	Fe-O	2.113

Table S5. Gibbs free energy for OER (eV).

	NiFe-LDH		NiFe-LDH/Fe-Ni ₂ P	
	Fe site	Ni site	Fe site	Ni site
ΔG_1	1.03	0.92	0.85	0.77
ΔG_2	0.70	0.75	0.74	0.67
ΔG_3	2.25	2.03	1.80	1.70
ΔG_4	0.94	1.23	1.52	1.78

Table S6. Solar-to-hydrogen performance of photovoltaic electrochemical catalyst systems.

Catalysts	Sorlar Cell	j_{OP}^* (mA cm ⁻²)	STH (%)	PCE (%)	STH/PCE (%)	Ref.
(-)Fe-NiP@NF Fe-NiP@NF(+)	PTB7-Th/PC ₇₁ BM/CO ₈ DFIC	30.38	5.57	7.62	73.1	This work
(-)NiFe LDH/Ni NiFe LDH/Ni(+)	CH ₃ NH ₃ PbI ₃	10	12.3	15.7	78.34	68
(-)NiMoZn NiBi(+)	4-cell c-Si	8.35	10.2	16	63.75	69
(-)Pt Ni(+)	Si	6.05	7.5	12.3	60.98	70
(-)CrNN NiFeLDH(+)	GaAs	12.1	14.9	20.18	73.84	71
(-)CoMnO@CN CoMnO@CN(+)	Si	6.43	8	16.1	49.69	72
(-)NiFeSP/NF NiFeSP/NF(+)	Si	7.5	9.2	28.5	32.28	73
(-)NiP Na _{0.08} Ni _{0.9} Fe _{0.1} O ₂ (+)	perovskite	9.12	11.22	14.69	76.38	74
(-)Ni–Pt Ni–Pt–Ni _{0.9} Fe _{0.1} O(+)	CIS perovskite	2.69 8.65	3.31 10.64	4.32 15.16	76.62 70.18	75
(-)NF NiFe(2:8)/NF(+)	c-Si	8.0	9.84	13.71	71.77	76

* Current density at operating condition.

References

- [1] H. Huang, C. Yu, C. Zhao, X. Han, J. Yang, Z. Liu, S. Li, M. Zhang, J. Qiu, *Nano Energy* **2017**, *34*, 472-480.
- [2] Y. Li, C. Zhao, *ACS Catal.* **2017**, *7*, 2535-2541.
- [3] W. Xu, S. Zhu, Y. Liang, Z. Cui, X. Yang, A. Inoue, *J. Mater. Chem. A* **2018**, *6*, 5574-5579.
- [4] Z. Liu, Y. Wang, R. Chen, C. Chen, H. Yang, J. Ma, Y. Li, S. Wang, *J. Power Sources* **2018**, *403*, 90-96.
- [5] Y. Gu, S. Chen, J. Ren, Y. Jia, C. Chen, S. Komarneni, D. Yang, X. Yao, *ACS Nano* **2018**, *12*, 245-253.
- [6] S. Zhao, M. Li, M. Han, D. Xu, J. Yang, Y. Lin, N. Shi, Y. Lu, R. Yang, B. Liu, Z. Dai, J. Bao, *Adv. Funct. Mater.* **2018**, *28*, 1706018.
- [7] C. Yuan, Z. Sun, Y. Jiang, Z. Yang, N. Jiang, Z. Zhao, U. Qazi, W. Zhang, A. Xu, *Small* **2017**, *13*, 1604161.
- [8] C. Gu, S. Hu, X. Zheng, M. Gao, Y. Zheng, L. Shi, Q. Gao, X. Zheng, W. Chu, H. Yao, J.

- Zhu, S. Yu, *Angew. Chem. Int. Ed.* **2018**, *57*, 4020-4024.
- [9] L. Yu, J. Yang, B. Guan, Y. Lu, X. Lou, *Angew. Chem. Int. Ed.* **2018**, *57*, 172-176.
- [10] G. Chen, Y. Zhu, H. Chen, Z. Hu, S. Hung, N. Ma, J. Dai, H. Lin, C. Chen, W. Zhou, Z. Shao, *Adv. Mater.* **2019**, *31*, 1900883.
- [11] J. Wang, L. Gan, W. Zhang, Y. Peng, H. Yu, Q. Yan, X. Xia, X. Wang, *Sci. Adv.* **2018**, *4*, eaap7970.
- [12] C. Wang, H. Yang, Y. Zhang, Q. Wang, *Angew. Chem. Int. Ed.* **2019**, *58*, 6099-6103.
- [13] Y. Shi, Y. Yu, Y. Liang, Y. Du, B. Zhang, *Angew. Chem. Int. Ed.* **2019**, *58*, 3769-3773.
- [14] C. Cao, D. Ma, Q. Xu, X. Wu, Q. Zhu, *Adv. Funct. Mater.* **2019**, *29*, 1807418.
- [15] N. Jiang, B. You, M. Sheng, Y. Sun, *Angew. Chem. Int. Ed.* **2015**, *54*, 6251-6254.
- [16] M. Ledendecker, S. Calderon, C. Papp, H. Steinrueck, M. Antonietti, M. Shalom, *Angew. Chem. Int. Ed.* **2015**, *54*, 12361-12365.
- [17] Y. Zhu, Y. Liu, T. Ren, Z. Yuan, *Adv. Funct. Mater.* **2015**, *25*, 7337-7347.
- [18] J. Duan, S. Chen, A. Vasileff, S. Qiao, *ACS Nano* **2016**, *10*, 8738-8745.
- [19] X. Wang, W. Li, D. Xiong, D. Petrovykh, L. Liu, *Adv. Funct. Mater.* **2016**, *26*, 4067-4077.
- [20] A. Sivanantham, P. Ganesan, S. Shanmugam, *Adv. Funct. Mater.* **2016**, *26*, 4661-4672.
- [21] J. Yu, Q. Li, Y. Li, C. Xu, L. Zhen, V. Dravid, J. Wu, *Adv. Funct. Mater.* **2016**, *26*, 7644-7651.
- [22] Y. Jin, H. Wang, J. Li, X. Yue, Y. Han, P. Shen, Y. Cui, *Adv. Mater.* **2016**, *28*, 3785-3790.
- [23] Y. Tan, H. Wang, P. Liu, Y. Shen, C. Cheng, A. Hirata, T. Fujita, Z. Tang, M. Chen, *Energy Environ. Sci.* **2016**, *9*, 2257-2261.
- [24] H. Liang, A. Gandi, D. Anjum, X. Wang, U. Schwingenschlogl, H. Alshareef, *Nano Lett.* **2016**, *16*, 7718-7725.
- [25] H. Shi, H. Liang, F. Ming, Z. Wang, *Angew. Chem. Int. Ed.* **2017**, *56*, 573-577.
- [26] C. Tang, R. Zhang, W. Lu, L. He, X. Jiang, A. Asiri, X. Sun, *Adv. Mater.* **2017**, *29*, 1602441.
- [27] L. Yu, H. Zhou, J. Sun, F. Qin, F. Yu, J. Bao, Y. Yu, S. Chen, Z. Ren, *Energy Environ. Sci.* **2017**, *10*, 1820-1827.
- [28] H. Zhang, X. Li, A. Haehnel, V. Naumann, C. Lin, S. Azimi, S. Schweizer, A. Maijenburg, R. Wehrspohn, *Adv. Funct. Mater.* **2018**, *28*, 1706847.
- [29] G. Chen, T. Wang, J. Zhang, P. Liu, H. Sun, X. Zhuang, M. Chen, X. Feng, *Adv. Mater.* **2018**, *30*, 1706279.
- [30] P. Menezes, C. Panda, S. Loos, F. Bunschei-Bruns, C. Walter, M. Schwarze, X. Deng, H. Dau, M. Driess, *Energy Environ. Sci.* **2018**, *11*, 1287.
- [31] Y. Li, H. Zhang, M. Jiang, Q. Zhang, P. He, X. Sun, *Adv. Funct. Mater.* **2017**, *27*, 1702513.
- [32] X. Lu, L. Yu, X. Lou, *Sci. Adv.* **2019**, *5*, eaav6009.
- [33] C. Xuan, Z. Peng, K. Xia, J. Wang, W. Xiao, W. Lei, M. Gong, T. Huang, D. Wang, *Electrochim. Acta* **2017**, *258*, 423-432.
- [34] W. Zhang, Y. Zou, H. Liu, S. Chen, X. Wang, H. Zhang, X. She, D. Yang, *Nano Energy*

2019, *56*, 813-822.

- [35] P. Wang, Z. Pu, Y. Li, L. Wu, Z. Tu, M. Jiang, Z. Kou, I. Arniinu, S. Mu, *ACS Appl. Mater. Interfaces* **2017**, *9*, 26001-26007.
- [36] M. Zhou, Q. Sun, Y. Shen, Y. Ma, Z. Wang, C. Zhao, *Electrochim. Acta* **2019**, *306*, 651-659.
- [37] Y. Ge, P. Dong, S. Craig, P. Ajayan, M. Ye, J. Shen, *Adv. Energy Mater.* **2018**, *8*, 1800484.
- [38] B. Weng, X. Wang, C. Grice, F. Xu, Y. Yan, *J. Mater. Chem. A* **2019**, *7*, 7168-7178.
- [39] G. Chen, T. Ma, Z. Liu, N. Li, Y. Su, K. Davey, S. Qiao, *Adv. Funct. Mater.* **2016**, *26*, 3314-3323.
- [40] B. You, Y. Sun, *Adv. Energy Mater.* **2016**, *6*, 1502333.
- [41] Y. Wu, G. Li, Y. Liu, L. Yang, X. Lian, T. Asefa, X. Zou, *Adv. Funct. Mater.* **2016**, *26*, 4839-4847.
- [42] C. Hu, L. Zhang, Z. Zhao, A. Li, X. Chang, J. Gong, *Adv. Mater.* **2018**, *30*, 1705538.
- [43] M. Wang, C. Ye, H. Liu, M. Xu, S. Bao, *Angew. Chem. Int. Ed.* **2018**, *57*, 1963-1967.
- [44] Y. Lin, K. Sun, S. Liu, X. Chen, Y. Cheng, W. Cheong, Z. Chen, L. Zheng, J. Zhang, X. Li, Y. Pan, C. Chen, *Adv. Energy Mater.* **2019**, *9*, 1901213.
- [45] C. Xing, Y. Xue, B. Huang, H. Yu, L. Hui, Y. Fang, Y. Liu, Y. Zhao, Z. Li, Y. Li, *Angew. Chem. Int. Ed.* **2019**, *58*, 13897-13903.
- [46] L. Yu, J. Zhang, Y. Dang, J. He, Z. Tobin, P. Kerns, Y. Dou, Y. Jiang, Y. He, S. Suib, *ACS Catal.* **2019**, *9*, 691-6928.
- [47] X. Huang, X. Xu, C. Li, D. Wu, D. Cheng, D. Cao, *Adv. Energy Mater.* **2019**, *9*, 1803970.
- [48] L. Huang, D. Chen, G. Luo, Y. Lu, C. Chen, Y. Zou, C. Dong, Y. Li, S. Wang, *Adv. Mater.* **2019**, *31*, 1901439.
- [49] X. F. Lu, L. Yu, J. Zhang, X. Lou, *Adv. Mater.* **2019**, *31*, 1900699.
- [50] R. Boppella, J. Tan, W. Yang, J. Moon, *Adv. Funct. Mater.* **2019**, *29*, 1807976.
- [51] M. Wang, W. Zhang, F. Zhang, Z. Zhang, B. Tang, J. Li, X. Wang, *ACS Catal.* **2019**, *9*, 1489-1502.
- [52] Y. Zhu, T. Ma, M. Jaroniec, S. Qiao, *Angew. Chem. Int. Ed.* **2017**, *56*, 1324-1328.
- [53] Y. Liu, Q. Li, R. Si, G. Li, W. Li, D. Liu, D. Wang, L. Sun, Y. Zhang, X. Zou, *Adv. Mater.* **2017**, *29*, 1606200.
- [54] T. Tang, W. Jiang, S. Niu, N. Liu, H. Luo, Y. Chen, S. Jin, F. Gao, L. Wan, J. Hu, *J. Am. Chem. Soc.* **2017**, *139*, 8320-8328.
- [55] L. An, J. Feng, Y. Zhang, R. Wang, H. Liu, G. Wang, F. Cheng, P. Xi, *Adv. Funct. Mater.* **2019**, *29*, 1805298.
- [56] Y. Pan, K. Sun, S. Liu, X. Cao, K. Wu, W. Cheong, Z. Chen, Y. Wang, Y. Li, Y. Liu, D. Wang, Q. Peng, C. Chen, Y. Li, *J. Am. Chem. Soc.* **2018**, *140*, 2610-2618.
- [57] E. Hu, Y. Feng, J. Nai, D. Zhao, Y. Hu, X. Lou, *Energy Environ. Sci.* **2018**, *11*, 872-880.
- [58] Q. Liang, H. Jin, Z. Wang, Y. Xiong, S. Yuan, X. Zeng, D. He, S. Mu, *Nano Energy* **2019**, *57*, 746-752.

- [59] T. Ouyang, Y. Ye, C. Wu, K. Xiao, Z. Liu, *Angew. Chem. Int. Ed.* **2019**, *58*, 4923-4928.
- [60] Z. Yang, C. Zhao, Y. Qu, H. Zhou, F. Zhou, J. Wang, Y. Wu, Y. Li, *Adv. Mater.* **2019**, *31*, 1808043.
- [61] T. Liu, P. Li, N. Yao, T. Kong, G. Cheng, S. Chen, W. Luo, *Adv. Mater.* **2019**, *31*, 1806672.
- [62] Z. Kang, H. Guo, J. Wu, X. Sun, Z. Zhang, Q. Liao, S. Zhang, H. Si, P. Wu, L. Wang, Y. Zhang, *Adv. Funct. Mater.* **2019**, *29*, 1807031.
- [63] Q. Hu, G. Li, G. Li, X. Liu, B. Zhu, X. Chai, Q. Zhang, J. Liu, C. He, *Adv. Energy Mater.* **2019**, *9*, 1803867.
- [64] Z. Chen, Y. Ha, H. Jia, X. Yan, M. Chen, M. Liu, R. Wu, *Adv. Energy Mater.* **2019**, *9*, 1803918.
- [65] C. Panda, P. Menezes, M. Zheng, S. Orthmann, M. Driess, *ACS Energy Lett.* **2019**, *4*, 747-754.
- [66] P. Xiong, X. Zhang, H. Wan, S. Wang, Y. Zhao, J. Zhang, D. Zhou, W. Gao, R. Ma, T. Sasaki, G. Wang, *Nano Lett.* **2019**, *19*, 4518-4526.
- [67] Y. Yang, H. Yao, Z. Yu, S. Islam, H. He, M. Yuan, Y. Yue, K. Xu, W. Hao, G. Sun, H. Li, S. Ma, P. Zapol, M. Kanatzidis, *J. Am. Chem. Soc.* **2019**, *141*, 10417-10430.
- [68] J. Luo, J. Im, M. Mayer, M. Schreier, M. Nazeeruddin, N. Park, S. Tilley, H. Fan, M. Graetzel, *Science* **2014**, *345*, 1593-1596.
- [69] C. Cox, J. Lee, D. Nocera, T. Buonassisi, *Proc. Natl. Acad. Sci. U. S. A.* **2014**, *111*, 14057-14061.
- [70] A. Landman, H. Dotan, G. Shter, M. Wullenkord, A. Houaijia, A. Maljusch, G. Grader and A. Rothschild, *Nat. Mater.* **2017**, *16*, 646-651.
- [71] M. Gong, W. Zhou, M. Kenney, R. Kapusta, S. Cowley, Y. Wu, B. Lu, M. Lin, D. Wang, J. Yang, B. Hwang, H. Dai, *Angew. Chem. Int. Ed.* **2015**, *54*, 11989-11993.
- [72] J. Li, Y. Wang, T. Zhou, H. Zhang, X. Sun, J. Tang, L. Zhang, A. Al-Enizi, Z. Yang, G. Zheng, *J. Am. Chem. Soc.* **2015**, *137*, 14305-14312.
- [73] Y. Xin, X. Kan, L. Gan, Z. Zhang, *ACS Nano* **2017**, *11*, 10303-10312.
- [74] B. Weng, F. Xu, C. Wang, W. Meng, C. Grice, Y. Yan, *Energy Environ. Sci.* **2017**, *10*, 121-128.
- [75] S. Kim, T. Kim, S. Lee, S. Baek, T. Park, K. Yong, *Adv. Mater.* **2017**, *29*, 1702431.
- [76] Y. Kim, J. Kim, Y. Jo, J. Lee, *ACS Catal.* **2019**, *9*, 9650.